NANO LETTERS

Communication

Metal-oxide Nanoparticle Mediated Enhanced-Raman Scattering and its Use in Direct Monitoring of Interfacial Chemical Reactions

Li Li, Tanya Hutter, Alex Finnermore, Fu Min Huang, Jeremy J Baumberg, Stephen Elliot, Ullrich Steiner, and Sumeet Mahajan

Nano Lett., **Just Accepted Manuscript** • Publication Date (Web): 05 Jul 2012

Metal-oxide Nanoparticle Mediated Enhanced-Raman Scattering and its Use in Direct Monitoring of Interfacial Chemical Reactions

*Li Li,[†] Tanya Hutter,[‡] Alexander S. Finnemore,[†] Fu Min Huang,[†] Jeremy J. Baumberg,[†] Stephen R. Elliott,[‡] Ullrich Steiner,[†] and Sumeet Mahajan[†]**

[†]Department of Physics, Cavendish Laboratory, University of Cambridge, Cambridge, CB3 0HE, UK. [‡]Department of Chemistry, University of Cambridge, Lensfield Road, Cambridge, CB2 1EW, UK.

KEYWORDS: Metal-oxide, plasmons, surface-enhanced Raman scattering, photocatalysis, interface

ABSTRACT: Metal-oxide nanoparticles (MONPs) have widespread usage across many disciplines but monitoring molecular processes at their surfaces *in situ* has not been possible. Here we demonstrate that MONPs give highly enhanced ($\times 10^4$) Raman scattering signals from molecules at the interface permitting direct monitoring of their reactions, when placed on top of flat metallic surfaces. Experiments with different metal-oxide materials and molecules indicate that the enhancement is generic and operates at the single nanoparticle level. Simulations confirm that the amplification is principally electromagnetic and is a result of optical modulation of the underlying plasmonic metallic surface by MONPs, which act as scattering antennae and couple

light into the confined region sandwiched by the underlying surface. Due to additional functionalities of metal oxides as magnetic, photo-electrochemical and catalytic materials, enhanced Raman scattering mediated by MONPs opens up significant opportunities in fundamental science, allowing direct tracking and understanding of application-specific transformations at such interfaces. We show a first example by monitoring the MONP-assisted photocatalytic decomposition reaction of an organic dye by individual nanoparticles.

Transition-metal oxides, due to the strong correlations of their *d* electrons, give rise to a wide variety of phenomena such as magnetism, ionic conduction, metal-insulator transitions, multiferroicity and superconductivity.[1] As a result, they have an extensivefrange of applications that include fuel cells, batteries, catalysts, sensors and microelectronics.[1] Despite the resulting importance of molecular binding and surface reactivity their utilization in plasmonic applications has been prevented by the tuning of their localized surface plasmon resonance (LSPR) into the infrared.[2-6] Surface-enhanced Raman scattering (SERS) is a popular plasmonic application utilizing ultraviolet (UV), visible (VIS) or near-infrared (NIR) excitation, which overcomes the extremely small scattering cross section (~10^{-30} cm^2 per molecule) in conventional Raman scattering[7] to yield a technique which offers non-invasive and non-destructive fingerprint characterization[8] with extensive applications in chemical and biological sensing. The amplification in SERS stems primarily from the electromagnetic (EM) enhancement (up to 10^{14})[9] obtained by excitation of SPR.[10] This is accompanied by typically smaller and system-dependent chemical enhancement as a result of formation of charge-transfer complexes between adsorbate and the surface.[11] Therefore, for efficient and sensitive SERS detection of molecules, nanoscale structures fabricated entirely with coinage metals (especially Ag and Au) have been the materials of choice since their SPR is easily excited in the VIS or NIR regions. On the other hand use of

metal-oxide nanoscale materials for enhanced Raman scattering has remained confined to few charge-transfer complexes,[12-14] limiting its widespread application to interfaces.

In this work, we demonstrate that Raman scattering can be greatly amplified just by placing metal-oxide nanoparticles (MONPs) on flat metallic surfaces. In order to differentiate this approach from the various metallic NP- (or NP array-) based SERS strategies,[15,16] we christen it **m**etal-**o**xide **n**anoparticle-**e**nhanced **R**aman **s**cattering (MONERS). Although its construction is analogous, it is unlike systems where the enhancements are due to coupling between the LSPR of the metallic NP and the propagating surface plasmon polaritons of the underlying metallic substrate[17,18] or the modification of LSPR modes of the plasmonic NP by dielectric substrate.[19,20] In this case the MONPs are non-plasmonic and do not have a LSPR in the wavelength range studied. Further, our method is generic, and applicable to a variety of MONPs fabricated from materials such as Fe_3O_4, TiO_2, WO_3 and ZnO. Advantages of using MONPs in comparison to metallic NPs are that they are abundant, less expensive, easily modified, biologically compatible and most importantly bring additional functionalities to the system. For example Fe_3O_4 NPs have been widely used in magnetically assisted bio-separations, controlled drug delivery and magnetic resonance imaging,[21] while TiO_2 NPs are widely used in nano-formulations such as sun-creams, and are of great interest for applications in dye-sensitized solar cells,[22] catalysis[23] and biosensors.[24] Probing enhanced Raman scattering signals by utilizing MONERS therefore opens up significant opportunities in a variety of fields involving metal-oxide materials and their interfaces. We demonstrate this by directly monitoring an interfacial chemical reaction and show an exemplar application utilizing the advantages of a MONERS system by tracking the photocatalytic decomposition of an organic dye mediated by TiO_2 NPs.

To demonstrate MONERS, we coated a monolayer of 4,4'-dimercaptostilbene (dithiol) on flat Au substrates and the respective NPs were then allowed to adsorb onto the monolayer, as illustrated schematically in Figure 1a. At the outset, we investigated Fe_3O_4 NPs (single Fe_3O_4 NPs; average diameter 254 ± 71 nm). The MONERS effect is generated at the single-particle level; to show this, the concentration of suspensions and the adsorption time were controlled such that the Fe_3O_4 NPs were well separated from each other (Fig. 1c). Figures 1d and e show, respectively, an SEM image and a MONERS image for a typical Fe_3O_4 NP on a dithiol-functionalized Au surface. Intense molecular signals are observed localized to the Fe_3O_4 NP spot only (Fig. 1e). Without the attachment of Fe_3O_4 NPs, no Raman signal from the dithiol was detected. To rule out the possibility that roughness might play a role in the enhancement, Au surfaces with a very high degree of flatness were prepared by a template-stripping method against mica.[25] These Au surfaces, with a root-mean-square (RMS) roughness of 0.3 nm, showed similar levels of enhancement to the normal flat Au surfaces fabricated by thermal evaporation (Supporting Information Fig. S1). Neither type of Au substrate showed any molecular signal in the absence of MONPs, confirming that Raman enhancements indeed only arise from the interaction between the MONPs and Au surfaces. Although we primarily discuss here the case where molecules have been adsorbed on the surfaces *before* NP attachment, the MONERS effect works equally well with molecules also adsorbed on NPs (Fig. 1b and data shown in Supporting Information Fig. S2).

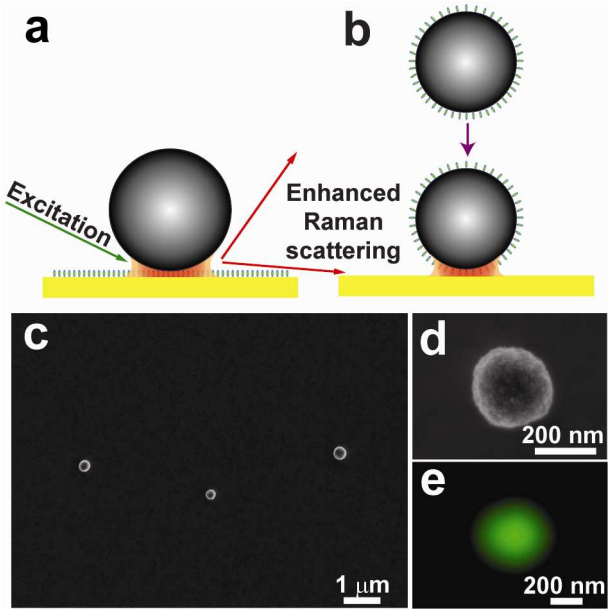

Figure 1. (a) Schematic of a MONP on a functionalized Au surface and (b) schematic of a functionalized MONP brought onto a bare Au surface. (c) A representative SEM image of well-separated Fe_3O_4 NPs. (d) An SEM image of an Fe_3O_4 NP; and (e) a MONERS image of an Fe_3O_4 NP on a dithiol-functionalized Au surface obtained by excitation with a 532 nm laser. The MONERS image is reconstructed by using the integrated intensities of the 1581 cm^{-1} peak and 1628 cm^{-1} peak of the dithiol molecule.

To explore the universality of the MONERS effect, we carried out experiments with a variety of MONPs (Table 1) in addition to the single Fe_3O_4 (sFe_3O_4) NPs mentioned above, each possessing a different crystalline structure (Supporting Information Fig. S3), band gap and refractive index (Supporting Information Table S1). MONERS spectra collected from different MONPs with the dithiol molecules on the surface are shown in Figure 2 (obtained with 532 nm laser excitation) and Supporting Information Figure S4 (obtained with 633 nm laser excitation), respectively. It is evident that all of these display the MONERS effect. This was again surprising, because some of these MONPs were irregularly shaped and a few of them formed agglomerates

(typically 100−400 nm; see Supporting Information Fig. S5). In the case of cFe_3O_4, WO_3 and ZnO, even though the particles used were clusters composed of small NPs, remarkably large MONERS signals were still observed from molecules on the Au surface. Strong MONERS signals were also obtained with TiO_2-rutile NPs as well as TiO_2-anatase and the commercially available TiO_2-P25 (Degussa) NPs (data not shown). In all the MONERS spectra shown in Figure 2, four distinct vibrational modes of dithiol are clearly observed, at 1078 cm^{-1} (ring mode-7a), 1186 cm^{-1} (ring mode-9a), 1581 cm^{-1} (ring mode-8b) and 1628 cm^{-1} ($\nu_{(C=C)}$).[26] In addition to the vibrational modes of dithiol, some bands are also observed below 900 cm^{-1}. These are characteristic of the MONPs used and are attributed to various phonon modes of the metal oxides, as also confirmed by the bulk Raman spectra collected from the corresponding MONP powders (Supporting Information Fig. S6).

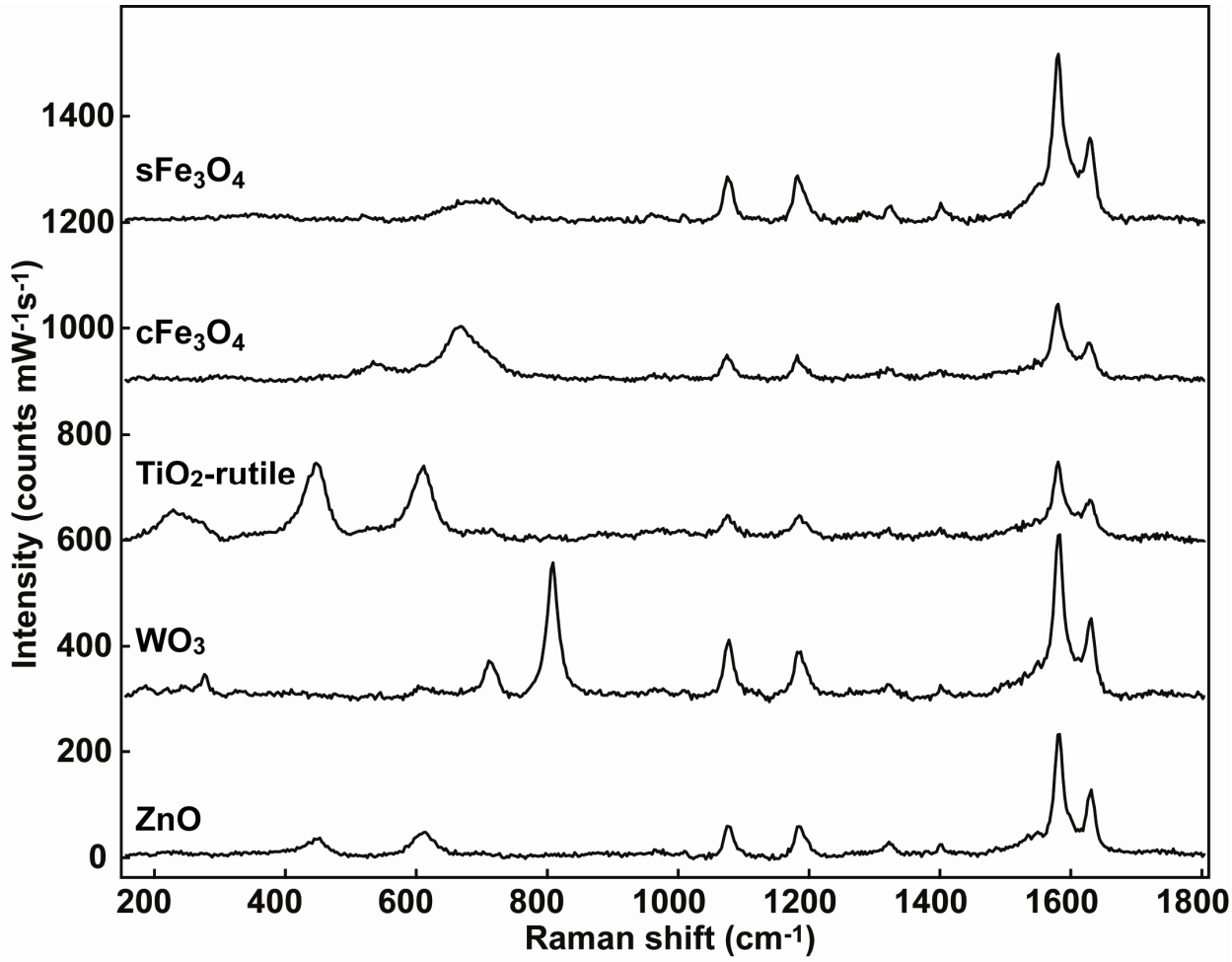

Figure 2. The MONERS spectra from single NP Fe_3O_4 (sFe_3O_4) as well from a cluster composed of smaller NPs of Fe_3O_4 (cFe_3O_4), TiO_2-rutile, WO_3 and ZnO on dithiol-functionalized Au surfaces with 532 nm excitation. The backgrounds have been subtracted and the spectra are offset for clarity.

The enhancements obtained in the MONERS system were typically 3−4 orders of magnitude compared to corresponding normal Raman measurements (Table 1). These are comparable to or higher than what has been achieved from nanostructured transition metals themselves,[27,28] for which reported enhancement values range between 10 and 10^4. The reported enhancements obtained for the transition metals, Fe (×1942)[29] and Zn (×221),[30] are lower than the

enhancements with MONERS. This is due to the higher absorption (inter-band transitions) in the VIS and NIR regions in transition metals compared to the transition-metal oxides investigated here. Although the enhancements are lower than in an analogous AuNP-on-Au system (Table 1 and Supporting Information Figs. S7 and S8),[17,18] they are sufficiently intense to give high signal-to-noise ratios in MONERS spectra (Fig. 2). Signals could be repeatedly recorded from the same NP more than 50 times under conditions below the degradation threshold. Variations in enhancement factors (EFs) across all systems are a manifestation of nanoscale differences in size, shape and nanoscale geometry. Nevertheless, given the large enhancements, especially compared to transition-metal nanostructures and the multi-functional aspects of metal oxides, MONERS holds enormous potential to study interfacial phenomena.

Table 1. Average experimental EFs for various NP-dithiol-Au systems.[a]

NPs	EF $\times 10^3$ (532 nm)	EF $\times 10^3$ (633 nm)	n (633 nm)
sFe_3O_4 (250 nm)	7.3 ± 6.0	17 ± 14	2.35 [31]
cFe_3O_4 (22 nm)	3.9 ± 2.7	9.7 ± 7.6	2.35 [31]
TiO_2-rutile	4.2 ± 3.2	23 ± 15	2.49 [32]
WO_3	7.7 ± 5.9	4.5 ± 5.2	2.10 [33]
ZnO	4.3 ± 5.3	2.5 ± 3.6	1.99 [34]
100 nm AuNP	150 ± 160	6400 ± 5200	

[a] Data were collected from 30−50 different NP spots. The 8b band (1581 cm^{-1}) of the dithiol is used for calculating the EF values. The refractive indices have been taken from the literature.

In order to interpret the observed results in terms of an EM mechanism, finite-element simulations (using the COMSOL Multiphysics software package) were carried out on the Fe_3O_4

NP on Au system with a gap distance of 1.3 nm, corresponding to the presence of the dithiol molecule.[35] Because of the weak spectral dependence, we consider enhancements in SERS from the quantity E^4, where E denotes $|E_y/E_0|$. Here, E_y refers to the localized scattered field in the y-direction mid-way in the gap between the NP and the Au surface (Supporting Information Fig. S9) and E_0 refers to the field in absence of the particle. We used three laser sources (λ_{ex}) in our experiments, at 532 nm, 633 nm and 785 nm. For a 200 nm Fe_3O_4 NP, the simulated $|E_y/E_0|^4$ is highest for 633 nm excitation and lowest for 785 nm excitation (Supporting Information Fig. S10). This is indeed consistent with the observed experimental EFs of the sFe_3O_4 MONERS system under excitation with different wavelengths (Supporting Information Fig. S10). However the broad MONERS resonance is effective over a much wider wavelength range than traditional plasmonic enhancements.

Figure 3a and Supporting Information Figure S11 display the effect of the NP size on the enhancement over the VIS-NIR range in the Fe_3O_4 NP-Au system under a p-polarized field at angles of incidence of 45° and 0° to the surface normal, respectively. Clearly, the enhancements increase with increasing NP diameter up to 300 nm and then show a slight decrease. This is due to an increase in the scattering cross-section with size, which, after a critical size, is radiatively damped due to depolarization effects across the particle.[36] The simulated scattering cross-section at a 45° angle of incidence for 200 nm Fe_3O_4 NPs is overlaid on the measured dark-field scattering spectra in Figure 3b. There is a good correspondence between them, as the size of the Fe_3O_4 NPs used here is of the order of 200 nm. The red shift observed with increasing Fe_3O_4 NP size is very similar to the well-known size dependence of SPR wavelengths found in all metallic NP systems.[37]

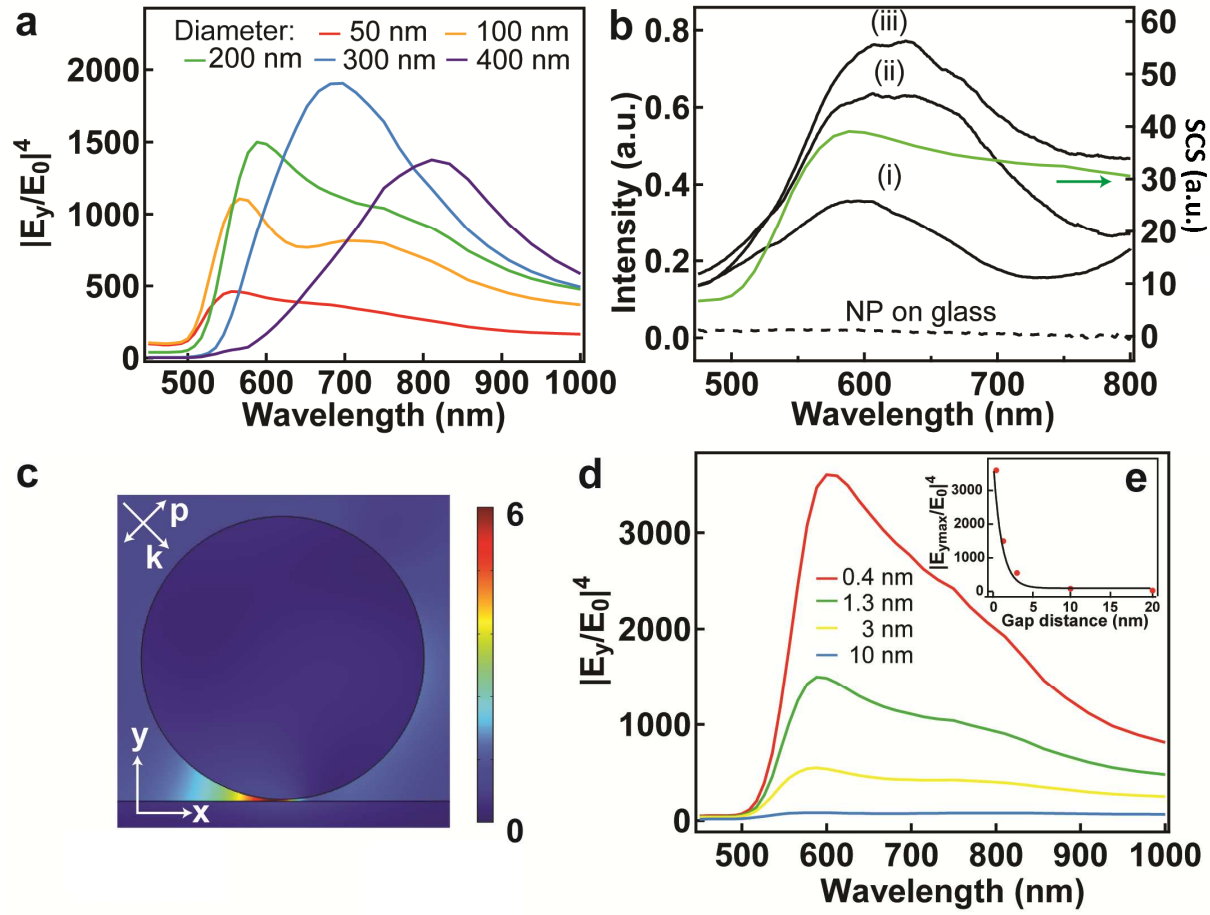

Figure 3. (a) Simulations of the NP size dependence of $|E_y/E_0|^4$; the gap distance is 1.3 nm. (b) Dark-field scattering spectra (i-iii) of three representative Fe_3O_4 NPs on Au and on glass overlaid with a simulated spectrum (green). (c) Simulated $|E_y/E_0|$ distribution at 633 nm around a 200 nm Fe_3O_4 NP on Au with a gap distance of 1.3 nm with 633 nm excitation. (d) Simulated spectral variation of $|E_y/E_0|^4$ for various values of gap distance. (e) $|E_{ymax}/E_0|^4$ of a 200 nm Fe_3O_4 NP on Au as a function of d/R, which can be fitted by a power-law function (black curve).[38] *p*-polarized light at an incident angle of 45° was used.

The simulation results indicate that the observed enhancement in MONERS is indeed due to optical modulation from the local dielectric perturbation by the MONPs. When a Fe_3O_4 NP is brought very close to the Au surface, the local dielectric constant is altered due to an EM

interaction with the continuum of delocalized propagating surface plasmons at the underlying Au surface, leading to a localization of the electric field in the gap formed between the NP and the metal surface. An alternative view considers enhanced scattering by the high-index NP exciting surface plasmons on a flat Au surface, which become confined in the gap, producing a large EM-field enhancement. While coupling to flat metal surfaces is impossible due to the momentum mismatch between the wave-vectors of a free-space photon and a plasmon confined to a surface, the high-index NP acts as an antenna coupling light into the gap above the metal surface. Although electric dipoles[39] and array of dielectric spheres[40] near a metallic surface as well the case of a metal NP on a high dielectric substrate[19] have been predicted to enhance scattering, the coupling and enhancement with a high refractive index MONP on a plasmonic surface is uniquely examined here.

The evidence that indeed excitation of localized surface plasmons of the substrate occurs on bringing MONPs close to the surface is seen in experiments with Pt which is only weakly plasmonic. Only a weak MONERS signal can be detected (data not shown) although thiols form well organized self-assembled monolayers on Pt similar to Au.[41] Clearly the size and type of NP material are important in MONERS but the plasmonic properties of the substrate are significant. A dielectric surface does not give any enhancement; Fe_3O_4 NPs on glass gave no enhancement and yield an MONERS EF of only ~23 in simulations (Supporting Information Fig. S12). Furthermore, by comparing the same vibrational modes of different molecules between Au NP on an Au surface and sFe_3O_4-based MONERS systems, we find consistent shifts in vibrational frequencies across all bands due to different chemical interactions but little difference in enhancements for the different peaks (Supporting Information Fig. S13). Also, the molecules mixed with MONPs alone do not produce any enhanced Raman signals (Supporting Information

Fig. S14). Therefore, we rule out a 'chemical effect' as a mechanism for the observed enhancements in MONERS.

The highest field enhancement is localized in the gap between the Fe_3O_4 NP and the Au substrate (Fig. 3c and Supporting Information Fig. S9). As expected, the enhancement effect in MONERS is highly sensitive to the size of the gap (Figs.3d,e). The distribution of E^4 becomes tighter and rapidly increases as the gap distance is decreased, due to higher field confinement and scales as $(d/R)^{1/2}$. Indeed, higher MONERS enhancements of 1.6 (± 1.7) × 10^5 were obtained with 4-mercaptobenzoic acid (MBA), where the MBA molecule is approximately half the length of the dithiol molecule. The intense enhancement obtained from MBA, along with many other dyes and molecules (Supporting Information Fig. S15), also proves that the enhancements demonstrated here show no selectivity towards probe molecules, unlike the charge-transfer enhancement observed for semiconductor NPs by other researchers.[12-14]

Significantly, no MONERS signals were obtained with dielectric particles, such as SiO_2 and polystyrene, under our experimental conditions. Simulations reveal that such SiO_2 NP-based MONERS system should indeed give two orders of magnitude lower enhancements (Supporting Information Fig. S16). This difference between Fe_3O_4 NP and SiO_2 NP systems indicates that the field enhancement is influenced by the refractive index of the NP. The correlation between refractive indices and EFs at 633 nm is evident since the observed MONERS EFs of ZnO and WO_3 are indeed lower than those of TiO_2-rutile and Fe_3O_4 (Table 1). This is consistent with our explanation that a higher refractive index NP leads to more efficient scattering with better confinement of the scattered field in the gap.

A key property of Fe_3O_4 NPs is that they are ferromagnetic and hence, are used in bio-separations. They assemble into linear chains under the influence of an external magnetic field (Fig. 4a). These chains are formed by single layer of Fe_3O_4 NPs. As clearly seen from Raman

map images (Fig. 4b) the intense signals are localized only to the assembled chains of NPs. Spectra obtained from MONERS chains under excitation from both 532 nm and 633 nm pump light (Figs.4c,d) show signals from molecules under the chains. This confirms the field enhancement is maximized in the gap between the particles and the surface, rather than between the particles themselves. This is further confirmed in simulations of a dimer on the surface (Fig. 4e and Fig. S17), which shows that field enhancements between the particles are very small compared to those in the gap between the particle and the substrate. In this case there is a very weak interaction between the MONPs themselves unlike metallic NPs which are plasmon active. Thus the ferromagnetic property in tandem with the MONERS approach could be used to separate and detect biomolecules *in situ* in solutions in real time.

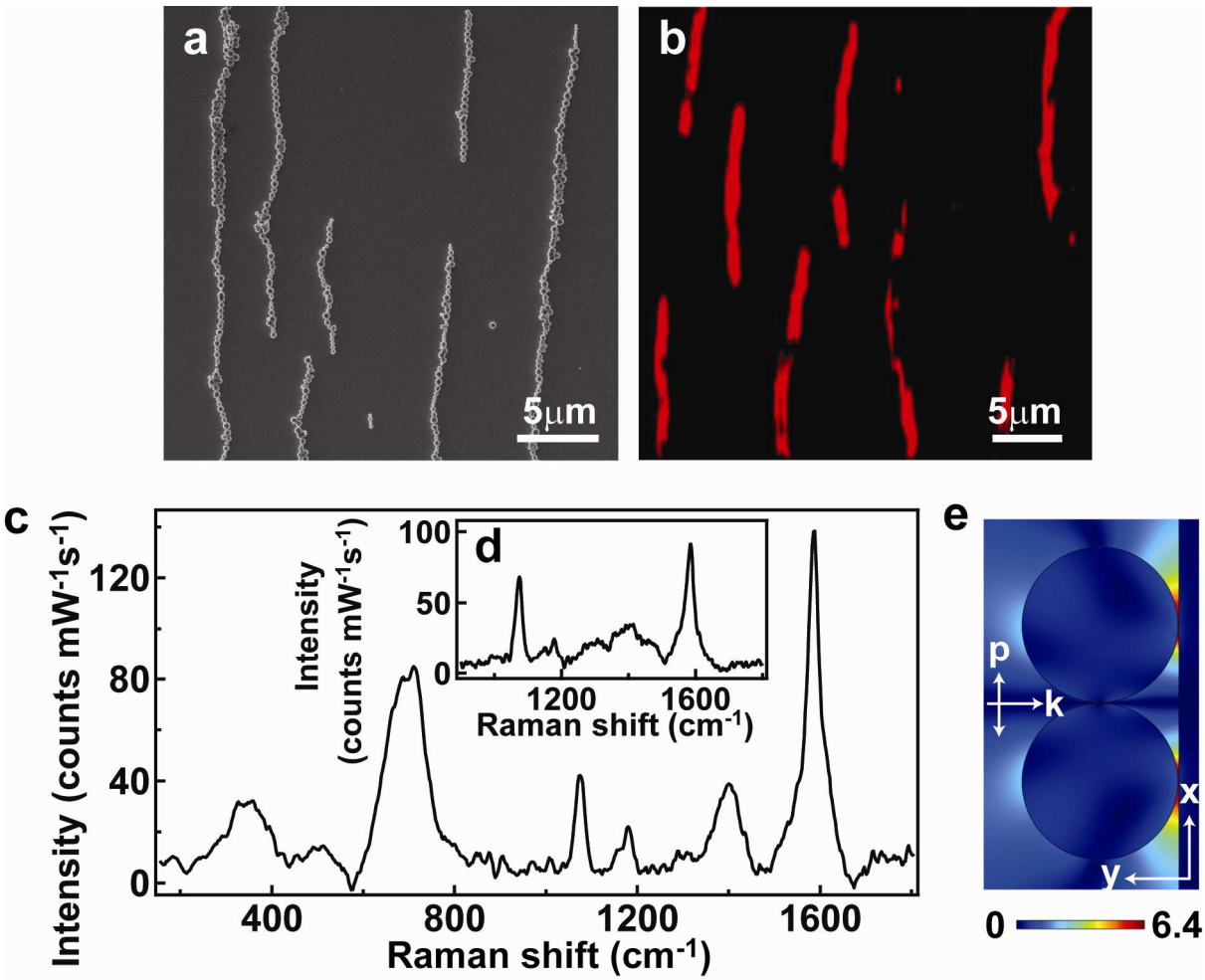

Figure 4. (a) An SEM image and (b) a MONERS image collected under excitation with a 633 nm laser of representative Fe_3O_4 lines assembled on an MBA-functionalized Au surface under the influence of an external magnetic field. The MONERS image is reconstructed by using the integrated intensities of the 1588 cm^{-1} peak of the MBA molecule. MONERS spectra from a spot on an Fe_3O_4 line on an MBA-functionalized Au surface under excitations with (c) 532 nm and (d) 633 nm lasers. The backgrounds have been subtracted. (e) Simulated $|E_y/E_0|$ distribution at 633 nm around a 200 nm diameter Fe_3O_4 NP dimer on Au under excitation with 633 nm at an incident angle of 0°. The gap distances between Fe_3O_4 NPs and between dimer and substrate are both 1.3 nm. E_y is the local field in the y direction; E_0 is the field in absence of the NP.

Furthermore, MONPs can not only assist in monitoring the molecular transformation at an interface but also actively catalyse it. We monitored the photocatalytic decomposition of methylene blue (MB) by TiO_2 NPs (P25, Degussa) by MONERS (Fig. 5). The spectra in Figure 5b clearly show that with increased exposure to UV radiation the characteristic Raman peaks of MB decrease in intensity. However, comparing the different Raman modes in the spectra the molecular mechanism can be elucidated. The 448 cm^{-1}, 500 cm^{-1}, 1510 cm^{-1} and 1624cm^{-1} are assigned to C−N−C, C−S−C, $-NH_2$ deformation and C−C ring stretching modes, respectively.[42] Figure 5c shows that the C−N−C bond is cleaved in preference to the C−S−C bond leading to a decrease in the ratio of the corresponding peaks. The simultaneous increase in the peak ratio of the $-NH_2$ deformation to the benzene ring mode agrees with the above and confirms predominant scission of the central ring *vis-a-vis* the adjacent benzene moieties, providing direct evidence of the degradation mechanism proposed for MB on TiO_2.[43] This clearly demonstrates that MONERS allows *direct* molecular observation and understanding of chemical processes at a metal-oxide interface.

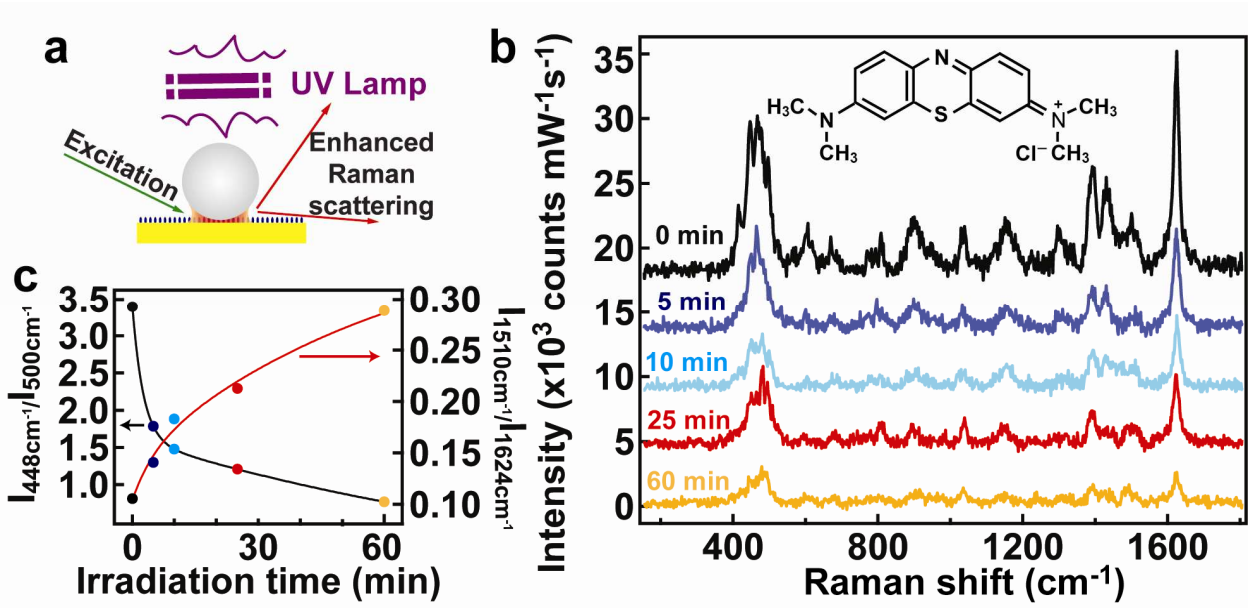

Figure 5. (a) Schematic of MONP mediated photocatalysis and simultaneous MONERS monitoring. (b) MB spectra after different exposures to UV irradiation showing rapid decrease of the peaks. MB molecular structure is shown in inset. (c) Ratio of intensities of the 448 cm^{-1} to the 500 cm^{-1} peaks decreases indicating predominant cleavage of C−N−C bond while that of 1510 cm^{-1} to the 1624 cm^{-1} peaks increases as a result of ring scission leading to formation of $-NH_2$.

In conclusion, the straightforward origin of the MONERS effect demonstrated here gives enhanced Raman scattering mediated by MONPs which has never been previously attempted. Although the construction is analogous to the metallic (Au or Ag) NP-on-substrate systems[17-20] it is fundamentally different since MONPs are non-plasmonic and the mechanism of coupling light into metallic surfaces is through optical effects induced by the high-index particle. This system can be similarly extended to other NPs with high refractive index, such us silicon and carbon NPs; further experiments are currently in progress. More importantly this work opens up a significant area for the fundamental and applied study of chemically-active surfaces not possible with the all metallic systems. We have shown initial proof-of-concept experiments to exemplify these distinct advantages, using MONPs to directly monitor and elucidate the mechanism of photocatalytic decomposition of MB. MONERS will thus aid understanding many types of interfacial phenomena, including those in catalysis and energy transfer in photovoltaics and photoelectrochemical systems, besides adding novel functionalities to traditional methods of detection and biosensing.

ASSOCIATED CONTENT

Supporting Information.

Experimental details; Figures S1-S17. This material is available free of charge via the Internet at http://pubs.acs.org.

AUTHOR INFORMATION

Corresponding Author

*E-mail: sm735@cam.ac.uk.

Notes

The authors declare no competing financial interest.

ACKNOWLEDGMENTS

We acknowledge funding from EPSRC (EP/H028757/1, EP/H007024/1, EP/G060649/1 and EU CUBIHOLES) for this work. We also thank Nokia Research Centre, Cambridge for studentship support (L. L.) and Trinity College Cambridge for a scholarship (T. H.).

REFERENCES

(1) Hwang, H. Y.; Iwasa, Y.; Kawasaki, M.; Keimer, B.; Nagaosa, N.; Tokura, Y. *Nature Mater.* **2012,** *11*, 103.

(2) Rhodes, C.; Franzen, S.; Maria, J.-P.; Losego, M.; Leonard, D. N.; Laughlin, B.; Duscher, G.; Weibel, S. *J. Appl. Phys.* **2006,** *100*, 054905.

(3) Li, S. Q.; Guo, P.; Zhang, L.; Zhou, W.; Odom, T. W.; Seideman, T.; Ketterson, J. B.; Chang, R. P. H. *ACS Nano* **2011,** *5*, 9161.

(4) Kanehara, M.; Koike, H.; Yoshinaga, T.; Teranishi, T. *J. Am. Chem. Soc.* **2009,** *131*, 17736.

(5) Losego, M. D.; Efremenko, A. Y.; Rhodes, C. L.; Cerruti, M. G.; Franzen, S.; Maria, J.-P. *J. Appl. Phys.* **2009,** *106*, 024903.

(6) Dominici, L.; Michelotti, F.; Brown, T. M.; Reale, A.; Di Carlo, A. *Opt. Express* **2009,** *17*, 10155.

(7) Nie, S.; Emory, S. R. *Science* **1997,** *275*, 1102.

(8) Cao, Y. C.; Jin, R.; Mirkin, C. A. *Science* **2002,** *297*, 1536.

(9) Kneipp, K.; Wang, Y.; Kneipp, H.; Perelman, L. T.; Itzkan, I.; Dasari, R. R.; Feld, M. S. *Phys. Rev. Lett.* **1997,** *78*, 1667.

(10) Moskovits, M. *Rev. Mod. Phys.* **1985,** *57*, 783.

(11) Otto, A. *J. Raman Spectrosc.* **2005,** *36*, 497.

(12) Musumeci, A.; Gosztola, D.; Schiller, T.; Dimitrijevic, N. M.; Mujica, V.; Martin, D.; Rajh, T. *J. Am. Chem. Soc.* **2009,** *131*, 6040.

(13) Tarakeshwar, P.; Finkelstein-Shapiro, D.; Hurst, S. J.; Rajh, T.; Mujica, V. *J. Phys. Chem. C* **2011,** *115*, 8994.

(14) Wang, X.; Shi, W.; She, G.; Mu, L. *Phys. Chem. Chem. Phys.* **2012,** *14*, 5891.

(15) Li, J. F.; Huang, Y. F.; Ding, Y.; Yang, Z. L.; Li, S. B.; Zhou, X. S.; Fan, F. R.; Zhang, W.; Zhou, Z. Y.; Wu, D. Y.; Ren, B.; Wang, Z. L.; Tian, Z. Q. *Nature* **2010,** *464*, 392.

(16) Li, J.-F.; Ding, S.-Y.; Yang, Z.-L.; Bai, M.-L.; Anema, J. R.; Wang, X.; Wang, A.; Wu, D.-Y.; Ren, B.; Hou, S.-M.; Wandlowski, T.; Tian, Z.-Q. *J. Am. Chem. Soc.* **2011,** *133*, 15922.

(17) Rycenga, M.; Xia, X.; Moran, C. H.; Zhou, F.; Qin, D.; Li, Z.-Y.; Xia, Y. *Angew. Chem. Int. Ed.* **2011,** *50*, 5473.

(18) Hill, R. T.; Mock, J. J.; Urzhumov, Y.; Sebba, D. S.; Oldenburg, S. J.; Chen, S.-Y.; Lazarides, A. A.; Chilkoti, A.; Smith, D. R. *Nano Lett.* **2010,** *10*, 4150.

(19) Knight, M. W.; Wu, Y.; Lassiter, J. B.; Nordlander, P.; Halas, N. J. *Nano Lett.* **2009,** *9*, 2188.

(20) Mubeen, S.; Zhang, S.; Kim, N.; Lee, S.; Krämer, S.; Xu, H.; Moskovits, M. *Nano Lett.* **2012,** *12*, 2088.

(21) Mornet, S.; Vasseur, S.; Grasset, F.; Duguet, E. *J. Mater. Chem.* **2004,** *14*, 2161.

(22) Guldin, S.; Hüttner, S.; Kolle, M.; Welland, M. E.; Müller-Buschbaum, P.; Friend, R. H.; Steiner, U.; Tétreault, N. *Nano Lett.* **2010,** *10*, 2303.

(23) Hoffmann, M. R.; Martin, S. T.; Choi, W.; Bahnemann, D. W. *Chem. Rev.* **1995,** *95*, 69.

(24) Zhou, H.; Gan, X.; Wang, J.; Zhu, X.; Li, G. *Anal. Chem.* **2005,** *77*, 6102.

(25) Hugall, J. T.; Finnemore, A. S.; Baumberg, J. J.; Steiner, U.; Mahajan, S. *Langmuir* **2012,** *28*, 1347.

(26) Osawa, M.; Matsuda, N.; Yoshii, K.; Uchida, I. *J. Phys. Chem.* **1994,** *98*, 12702.

(27) Tian, Z.-Q.; Ren, B.; Wu, D.-Y. *J. Phys. Chem. B* **2002,** *106*, 9463.

(28) Abdelsalam, M. E.; Mahajan, S.; Bartlett, P. N.; Baumberg, J. J.; Russell, A. E. *J. Am. Chem. Soc.* **2007,** *129*, 7399.

(29) Cao, P. G.; Yao, J. L.; Ren, B.; Mao, B. W.; Gu, R. A.; Tian, Z. Q. *Chem. Phys. Lett.* **2000,** *316*, 1.

(30) Gu, R.-A.; Shen, X.-Y.; Liu, G.-K.; Ren, B.; Tian, Z.-Q. *J. Phys. Chem. B* **2004,** *108*, 17519.

(31) Schlegel, A.; Alvarado, S. F.; Wachter, P. *J. Phys. C: Solid State Phys.* **1979,** *12*, 1157.

(32) Bass, M., *Handbook of optics, 3rd edition, Vol. IV: optical properties of materials, nonlinear optics, quantum optics*. McGraw-Hill: New York, 2009.

(33) Rao, M. C.; Hussain, O. M. *Res. J. Chem. Sci.* **2011,** *1*, 76.

(34) Bass, M., *Handbook of optics, 2nd edition, Vol. II: devices, measurements, and properties*. McGraw-Hill: New York, 1994.

(35) Guarrotxena, N.; Ren, Y.; Mikhailovsky, A. *Langmuir* **2011,** *27*, 347.

(36) Blaber, M. G.; Schatz, G. C. *Chem. Commun.* **2011,** *47*, 3769.

(37) Driskell, J. D.; Lipert, R. J.; Porter, M. D. *J. Phys. Chem. B* **2006,** *110*, 17444.

(38) Huang, F.; Baumberg, J. J. *Nano Lett.* **2010,** *10*, 1787.

(39) Xiao, M.; Zayats, A.; Siqueiros, J. *Phys. Rev. B* **1997,** *55*, 1824.

(40) Inoue, M. *Pure Appl. Chem.* **1987,** *59*, 1253.

(41) Love, J. C.; Estroff, L. A.; Kriebel, J. K.; Nuzzo, R. G.; Whitesides, G. M. *Chem. Rev.* **2005,** *105*, 1103.

(42) Hutchinson, K.; Hester, R. E.; Albery, W. J.; Hillman, A. R. *J. Chem. Soc., Faraday Trans. 1* **1984,** *80*, 2053.

(43) Houas, A.; Lachheb, H.; Ksibi, M.; Elaloui, E.; Guillard, C.; Herrmann, J.-M. *Appl. Catal. B: Environ.* **2001,** *31*, 145.

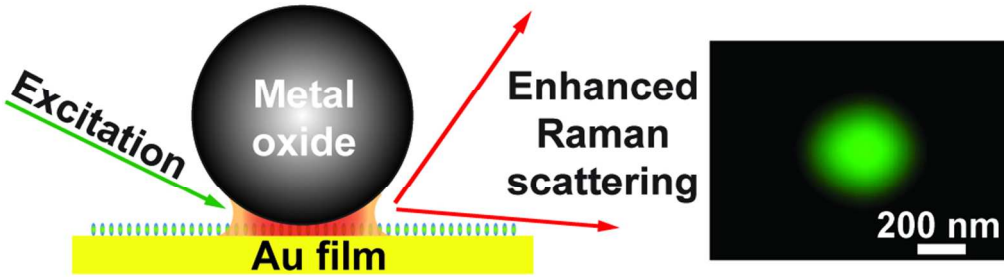

87x25mm (300 x 300 DPI)